BBC
BROWN BOVERI

Rotors for Large Steam Turbines

Publication No. CH-T 060 053 E

Rotors for Large Steam Turbines

A. Hohn

As the unit capacity of steam turbosets increases, so too does the size of the rotor, and hence also the stresses applied to it. The various designs of rotor are discussed and results of stress calculations given. Rotor materials are considered briefly, followed by comment on the future development of rotor design for large steam turbines.

Introduction

Steam turbines today are remarkable particularly for their size: unit capacities of more than 1000 MW are now to be found both in conventional power stations with fossil-fuelled boilers and also in nuclear power plant. For a number of reasons, unit capacities will rise even further in future, and it would be premature at the moment to speak of any limit. Machines of this size represent a substantial financial commitment and in the event of failure cause serious disruption of the power supply to both domestic and industrial users. It is therefore understandable that the manufacturer of such machines does as much as the latest state of the technology will allow in order to ensure that these large machines are reliable in service.

This article is concerned with the heart of the machine, the rotor, and reference is made to the various rotor designs and the differences between them. Full treatment of the subject would have to include the static behaviour in steady-state operation and under transient conditions, and also the dynamics of the rotor under the influence of the flow of steam. This, however, would go beyond the scope of an article, and therefore the main focus of attention here is on steady-state operation which at all events constitutes the basis of the mechanical design, and on which all other phenomena are superimposed.

Rotor Configurations

The designs current today are restricted to the forms shown in Fig. 1:

- Diagram a shows two rotors, each produced from a single forging.
- Shrinking discs on to a central shaft which transmits the torque gives rise to the composite construction of diagram b.
- In diagram c, separate discs have been welded together to form a drum-type rotor [1].

Each configuration has its own advantages and disadvantages as regards production of the steel, heat treatment, machining and testing, but these will not be dealt with specifically here. Distinctive differences in the matter of stresses are considered in the following two sections.

Statics of Rotors under the Influence of Speed, Disc Geometry and Temperature

The Disc under the Influence of Rotation

All designers of turbomachines use the rotating disc in one form or the other as a basic component of the rotor. The following remarks on the rotating disc, which are of an elementary nature and can be pursued further in [2, 3, 4] for example, are therefore applicable to all, with account taken of the boundary conditions particular to a specific design.

If the equilibrium of forces in the radial direction is taken on a rotating disc element of constant thickness, allowance is made for the relationship between radial and tangential expansion in the disc and Hooke's law for biaxial stress is introduced, we obtain the differential equation of the rotating disc in terms of σ_r with the general solution:

$$\sigma_r = C_1 + \frac{C_2}{r^2} - \frac{\varrho\,\omega^2\,(3+\nu)}{8}\,r^2$$

Disregarding any external tension for the time being, the curves of radial and tangential stress are found to be as follows for:

a. *a solid disc:*

$$\sigma_r = \frac{\varrho\,\omega^2\,(3+\nu)}{8}(r_2^2 - r^2) \qquad (2)$$

and since $\sigma_t = \frac{d}{dr}(r\,\sigma_r) + \varrho\, r^2\,\omega^2$

$$\sigma_t = \frac{\varrho\,\omega^2\,(3+\nu)}{8}\left(r_2^2 - \frac{1+3\nu}{3+\nu}\,r^2\right) \qquad (3)$$

b. *a perforated disc:*

$$\sigma_r = \frac{\varrho\,\omega^2\,(3+\nu)}{8}\left[r_1^2 + r_1^2 - \frac{r_1^2\,r_2^2}{r^2} - r^2\right] \qquad (4)$$

$$\sigma_t = \frac{\varrho\,\omega^2\,(3+\nu)}{8}\left[r_1^2 + r_2^2 + \frac{r_1^2\,r_2^2}{r^2} - \frac{1+3\nu}{3+\nu}\,r^2\right] \qquad (5)$$

In order to show equations (2) to (5) in general form they are made dimensionless with the stress prevailing at the centre of the solid disc, i.e. with $\sigma_r = \sigma_t = \varrho\, r_2^2\,\omega^2\,(3+\nu)/8$. The result can be seen in Fig. 2. To illustrate more clearly the mutual influences of radial and tangential stress, Fig. 2 also includes the dimensionless comparative stress S_V on the assumption of constant work of deformation, thus:

$$\sigma_V = \sqrt{\sigma_r^2 + \sigma_t^2 - \sigma_r\,\sigma_t} \qquad (6)$$

und $$S_V = \frac{8\,\sigma_V}{\varrho\, r_2^2\,\omega^2\,(3+\nu)} \qquad (7)$$

From Fig. 2 we can draw a first conclusion:

For the same dimension (r_2), the same material (ϱ) and the same speed (ω), the perforated disc will exhibit a

Fig. 1 – Different types of rotor construction

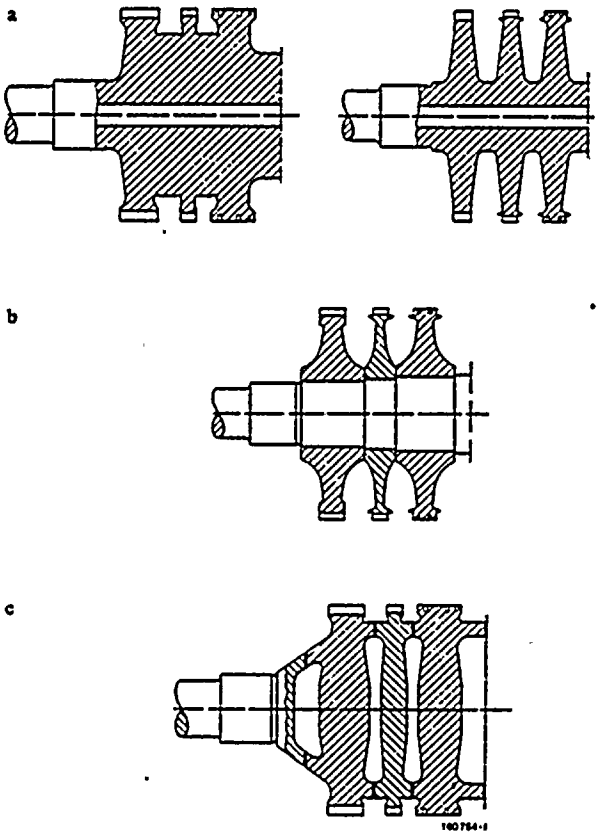

Fig. 2 – Dimensionless radial, tangential and combined stresses of discs of equal width

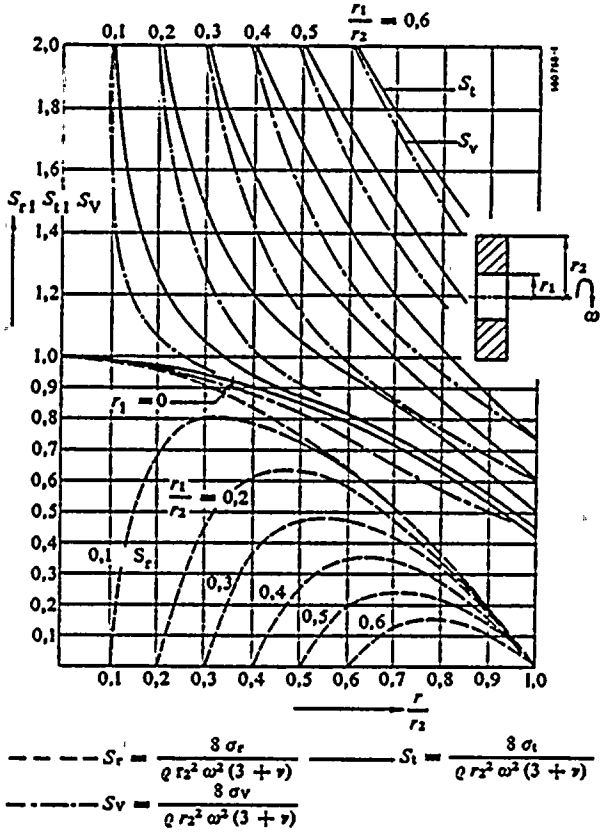

higher loading than the solid disc. A measure of this is the mean tangential stress.
This result also remains essentially unchanged when the additional loads caused by blade tension, steam pressure and shrinkage are superimposed on the rotational stresses.
The considerations presented so far are sufficient for determining the rotational stresses in the case of a solid disc. For the perforated and shrunk-on disc of Fig. 1b, however, deformation also has to be taken into account, owing to the different stiffness of the central shaft and the disc. Only then can one define the required degree of shrinkage, which in turn has an influence on the choice of material.

Deformation Affecting the Perforated Disc

Here we can again start from Eq. (1) and determine the integration constants C_1 and C_2 appropriate to the boundary conditions. With the aid of the calculated stresses it is possible to determine the radial expansion, and hence also the radial displacement U for any radius of the central shaft or of the shrunk-on disc. Of particular interest are the relative displacements U_1 of shaft and disc at the point of attachment with radius r_1. The result of considering deformation in this way can be read from the Table. Thus, any expansion of disc or shaft is proportional to the forces σ_{r1} and σ_{r2} which cause it. There is a square-law relationship between the expansion and rotation ω. Here it must be noted that for different speeds the external tension σ_{r2} also varies as the square of the speed. The shrunk-on body has to satisfy the following conditions: at the point of contact between disc and shaft at radius r_1 the sum of disc expansion and shaft compression must equal the degree of shrinkage Δr, i.e.

$$\Delta r = r_{1W} - r_{1S} = U_{1W} + U_{1S} \qquad (8)$$

With this it is now possible to construct a "spring diagram" of the shrunk joint (Fig. 3), and within this the relative degree of shrinkage $\Delta r/r$ can be determined for a given geometry (r_1, r_2) and a desired shrinkage force σ_{r1}. The shrinkage force is chosen in the light of the two following points:

– Expansion of the disc due to rotation may only be large enough to ensure that a positive fixing is maintained when run at overspeed (normally 1·2 × operating speed), i.e. the disc must not come loose. Publications by manufacturers of this type of construction indicate that the lift-off speed (zero-shrinkage) lies approximately 35% above the normal operating speed [5].
– It must also be ascertained whether, at normal operating speed, the shrunk-on disc is fully capable of transferring the blade torque to the central shaft. Generally speaking, this requirement is always met if the overspeed condition is satisfied.

Our considerations regarding the shrunk-on disc can thus be summarized as follows:
At standstill the disc is stretched because it was undersize when fitted on the shaft, and the shaft is compressed by the shrinkage. Owing to its own rotation and the tensile force exerted by the blades the disc expands *more* than the central shaft. The shrinkage force is thus reduced. A residual degree of shrinkage must be retained when the rotor is run at overspeed.

Expansion of shaft and disc

	Shrinkage force	Rotation	External tension
	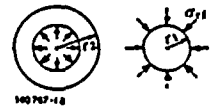	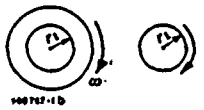	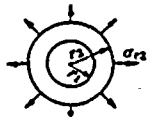
Shaft	$\left(\frac{U_1}{r_1}\right)_{W\sigma_{r1}} = \frac{\sigma_{r1}}{E}(1-\nu)$	$\left(\frac{U_1}{r_1}\right)_{W\omega} = \frac{\varrho r_1^2 \omega^2 (1-\nu)}{4E}$	—
Disc	$\left(\frac{U_1}{r_1}\right)_{S\sigma_{r1}} = \frac{\sigma_{r1}}{E} \cdot \frac{r_1^2}{r_2^2 - r_1^2} \times \times \left[(1-\nu) + \frac{r_2^2}{r_1^2}(1+\nu)\right]$	$\left(\frac{U_1}{r_1}\right)_{S\omega} = \frac{\varrho r_1^2 \omega^2}{4E} \times \times \left[\frac{r_2^2}{r_1^2}(3+\nu) + (1-\nu)\right]$	$\left(\frac{U_1}{r_1}\right)_{S\sigma_{r2}} = 2\frac{\sigma_{r2}}{E} \cdot \frac{r_2^2}{r_2^2 - r_1^2}$

Figure 3 shows these relationships for standstill ($\omega = 0$), operating speed (ω), overspeed ($\omega = \omega'$) and lift-off speed ($\omega^* = 1{\cdot}35\,\omega$) for a disc of uniform width with a radius ratio of $r_2/r_1 = 3$. In this diagram the elasticity properties of the disc and the central shaft have been determined in accordance with the Table. On the abscissa the point of origin is the desired degree of shrinkage $(\Delta r/r_1)_0$, which is selected according to the residual shrinkage (ordinate) desired at the overspeed condition. The individual components of the disc and shaft expansion due to rotation and external tension σ_{r2} have also been taken from the Table. In order to establish the order of magnitude of the compressive forces σ_{r1} involved, and also the residual shrinkage, the diagram was compiled using realistic conditions such as occur in the case of l.p. rotors for half-speed steam turbines: $n = 1500$ rev/min, equivalent to $\omega = 157\ s^{-1}$; overspeed $\omega' = 1{\cdot}2\ \omega$; blade tension σ_{r2} being taken as 8 kgf/mm² at the normal operating speed. The residual shrinkage for any speeds can be obtained directly from Fig. 3 by means of the following conversion from the stationary shrinkage diagram. The basic principles of this are explained in [6].

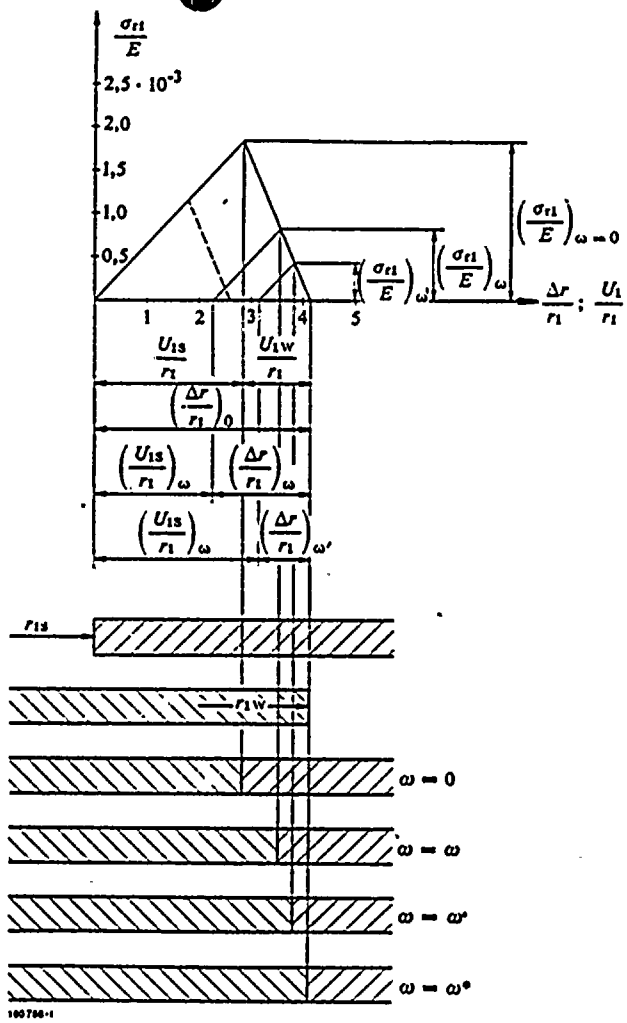

Fig. 3 – Shrinkage diagram for shrunk-on discs under different operating conditions

We have:

$$\left(\frac{\Delta r}{r_1}\right)_0 : \left(\frac{U_{1S}}{r_1}\right)_\omega = \left(\frac{\omega^*}{\omega}\right)^2 \tag{9}$$

Since the residual shrinkage Δr_ω at operating speed ω is given by

$$\left(\frac{\Delta r}{r_1}\right)_\omega = \left(\frac{\Delta r}{r_1}\right)_0 - \left(\frac{U_{1S}}{r_1}\right)_\omega \tag{10}$$

for the residual shrinkage we obtain

$$\left(\frac{\Delta r}{r_1}\right)_\omega = \left(\frac{\Delta r}{r_1}\right)_0 \cdot \left[1 - \left(\frac{\omega}{\omega^*}\right)^2\right] \tag{11}$$

Thus it can be seen from Fig. 3 that an extremely large degree of shrinkage ($4{\cdot}15 \times 10^{-3}$) is necessary to achieve a lift-off speed of $\omega^* = 1{\cdot}35\ \omega$, taking into account the blade tension.

If for the example in Fig. 3 it had been stipulated that lift-off is to occur at 135% of operating speed *without* allowance for the external tension σ_{r2} (i.e. without blading), this would result in the standstill shrinkage diagram shown by the broken line in Fig. 3, with a standstill shrinkage of $2{\cdot}6 \times 10^{-3}$. In this case, however, the bladed rotor would lose its residual shrinkage even at small overspeeds (9% in this instance), owing to the blade tension, and some means such as keys would be needed to prevent the disc from slipping. The reserve of speed up to lift-off mentioned here is determined by the residual shrinkage obtained with Eq. (11).

Influence of Disc Geometry

The above statements are of a fundamental nature and aid one's understanding when comparing different designs. But in practice the shrunk-on disc is not of constant width. The disc meridian will therefore be shaped in some way, it will be formed to yield a disc of uniform strength or the perforated disc will be given a hyperbolic meridian similar to $y = c/r^n$, in order to make the best possible use of the material. This then results in a more gentle disc characteristic than shown in Fig. 3, and hence in a reduction of the necessary shrinkage force. But here, too, a very tight shrink fit will still be needed for a great variety of disc meridian shapes, which is one reason why highly tempered materials are chosen for the discs.

There are a number of methods (e.g. [2]) for calculating the stress in a disc of any technically feasible contour. The method of finite elements has recently come to be used for this purpose, even going to the extent of not only determining the stress conditions in the individual parts (discs) of the rotor, but also of considering the rotor as an entity and taking into account the interactions between neighbouring parts of the discs. A very good overall investigation of the rotor is always possible with the method of finite elements, the fundamentals of which can be found described in [6]. Detailed investigations,

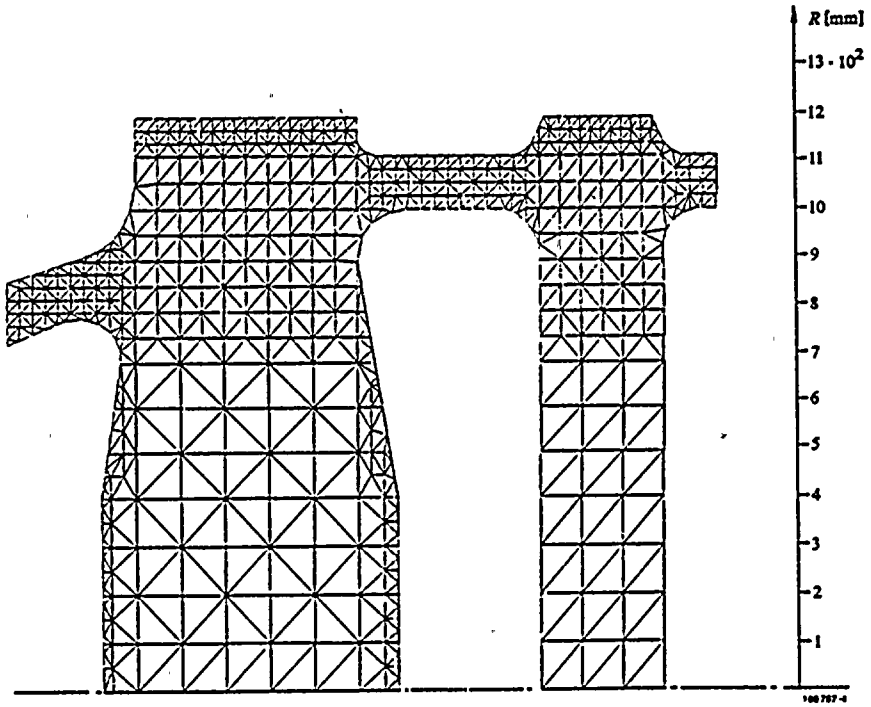

Fig. 4 – Grid for calculating stresses in a l.p. rotor by the finite element method

such as in the slots of blade fixings, need more refined calculation applied over a very fine grid, while the aid of photoelastic techniques must be enlisted for assessing the surface stress in the grooves. In this manner one can account for all the stress components involved.

Influence of Temperature

Under normal operating conditions the rotors of large steam turbines are in general exposed to a steady-state temperature field: after start-up and settling down to normal load an isothermal distribution becomes established in the respective rotors which varies only slightly in response to moderate load fluctuations.
A knowledge of the isotherm distribution in the rotor is necessary for two reasons:

– first, one needs to know the local temperature in order to compare the local stress present with the characteristic of the material (e.g. long-time strength) valid at this local temperature,
– second, the isothermal condition gives rise to a stress field which it may be important to calculate for the total loading on the rotor.

This raises the question of how one determines the isotherm distribution in the rotor. Basically this is a problem of thermal conduction [7] in a rotationally symmetrical body described by the Fourier equation

$$\frac{\partial T}{\partial t} = a^2 \Delta T \qquad (12)$$

where $a^2 = \dfrac{\lambda}{c\varrho}$ (13)

Before setting about solving this equation one must know the boundary conditions, e.g. surface temperature, heat supplied and removed.
In practice, the rotor geometry does not follow a simple shape and the temperature distribution at the surface is complex, owing the cooling effect of the steam. Consequently, one cannot expect a complete solution to the heat conduction equation. There are nevertheless two practical ways of solving this problem:

– The isotherms in the rotor are found with the aid of an electrical analogue model, in which case the rotational symmetry of the rotor is accounted for by selecting suitable resistances (perforations) on the two-dimensional model.
The conduction of an electrical current through a body is described by the equation

$$\frac{\partial U}{\partial t} = \frac{\varkappa}{C} \Delta U \qquad (14)$$

and is thus analogous to the heat conduction equation (12). Here, U is the applied voltage, C the electrical capacitance and $\varkappa$ the electrical conductivity of the material. Lines of equal voltage U, or equal potential, are an analogue of the isotherms T = constant.

– Another possible way of determining the temperature distribution in the rotor is to solve the heat conduction equation by numerical methods. This possibility has gained greatly in significance in recent years with the use

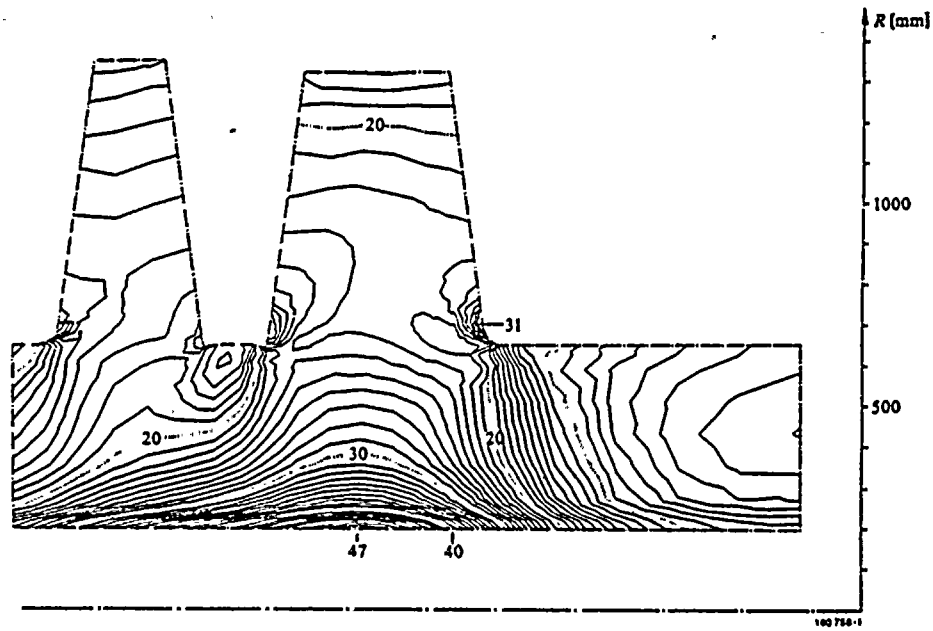

Fig. 5 – Von Mises' combined stress field of the solid l.p. rotor shown in Fig. 1a

Values 20 to 47 kgf/mm².

of finite elements for calculating stress. One has the advantage that the results of calculating temperature in this way lie on the same lattice as the subsequent stress calculation, and thus can be used as a direct input for computing the termal stress.

Finally, as regards determining the isotherms it must be said that without the subsequent stress calculation it will always be fragmentary and yield only moderately useful information.

Practical Results of Stress Calculations

Rotational Stresses in Different LP Rotor Designs

The discussion in the previous section on stress calculation in rotors of different constructions is now illustrated below with the aid of a few practical examples.

Figure 4 shows the grid imposed on a l.p. rotor for determining the mechanical stresses by the finite element method. All the basic designs depicted in Fig. 1 were calculated in a similar manner.

When computing the stresses, the speed and blade tension were kept constant for all types of rotor. Shape, dimensions, speed and blade tension correspond to values found in practice.

Figure 5 illustrates the comparative stress field for a l.p. rotor machined from the solid as shown in Fig. 1a. Here the comparative stress has been taken as according to von Mises:

$$\sigma_V = \frac{1}{\sqrt{2}} \cdot \sqrt{(\sigma_r - \sigma_t)^2 + (\sigma_t - \sigma_z)^2 + (\sigma_z - \sigma_r)^2 + 6\sigma_{rz}^2} \quad (15)$$

It will be seen that owing to the abrupt change of cross-section from the central shaft portion to the disc, stress concentrations as high as 31 kgf/mm² occur. Stress concentrations of this kind are always to be found when the force field is disturbed as a result of changes in cross-section. Fig. 5 also shows the stress level at the inner bore, with a radius ratio of $r_1/r_2 = 0{\cdot}15$. At 47 kgf/mm² the stress here reaches a very high value, although it is still always below that of shrunk-on discs. Results of calculating the stresses in shrunk-on discs are shown in Fig. 6. Owing to the larger central bore for the shaft a much higher stress of 68 kgf/mm² is found here, otherwise the conditions are the same as in Fig. 5. At the transition from the slim part of the disc to the broad outer shoulder one can again see a stress concentration in the corner of the divergence, attaining local values of 70 to 80 kgf/mm² and caused chiefly by disruption of the radial stress pattern.

A technique often used in the past was to secure the shrunk-on discs with extra keys. This inevitably gives rise to stress concentrations in the keyway which in the most favourable case have a stress concentration factor of about three. What this means with the high basic stress level of a perforated disc is easy to appreciate: from the start a plastic zone will form round the slot which, if the properties of the material are less than ideal, can lead to cracking and hence to failure of the disc when it is rotating. Sufficient instances of this have unfortunately occurred in the past [9, 10]. In order to meet the standards of reliability required in power stations, therefore, it is essential that no keys of any kind should be provided as an extra means of securing the discs.

As already explained in connection with Fig. 2, the solid disc will show the most favourable stress characteristics.

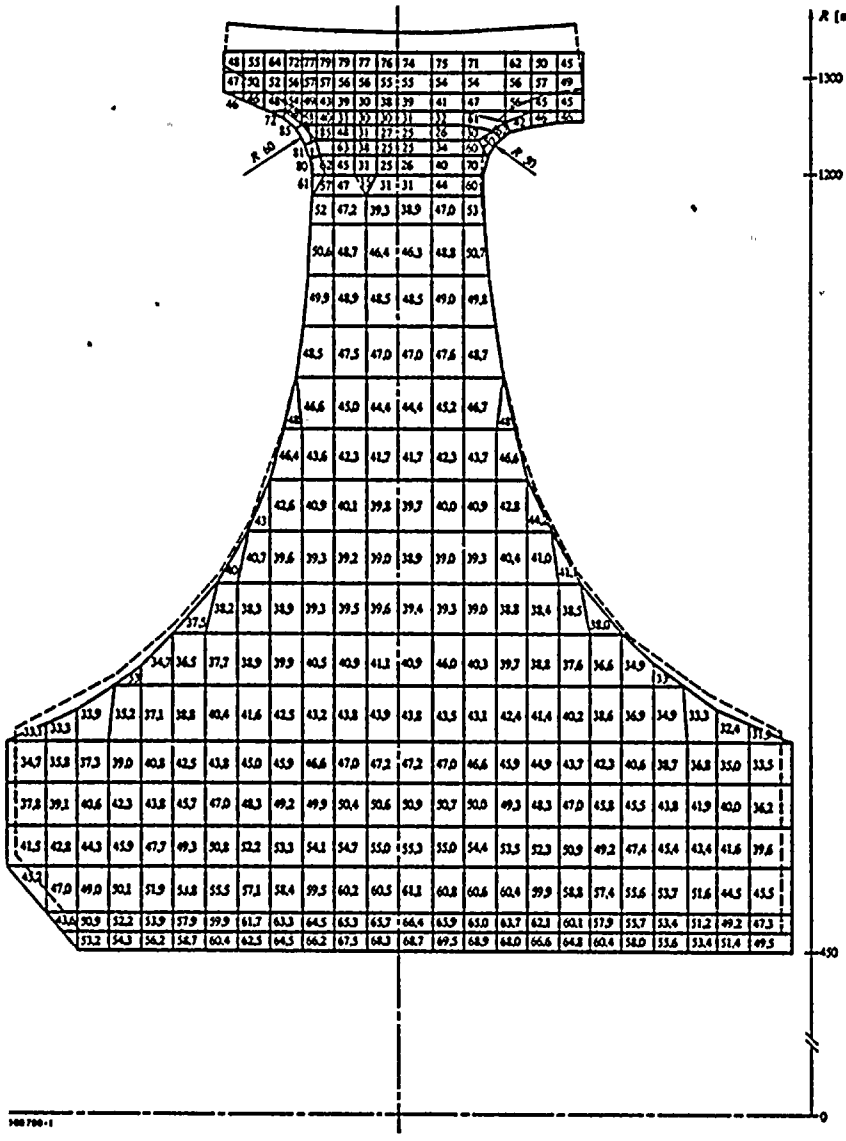

Fig. 6 – Combined stress field of a l.p. disc rotor as shown in Fig. 1b, in kgf/mm²

Figure 7 illustrates the combined stress distribution (after von Mises) in a welded drum rotor of a type found in machines of over 1000 MW. The boundary conditions – outside diameter and blade tension – are comparable with the designs shown in Fig. 5 and 6, the speed being taken as 1800 rev/min in all the cases shown. It will be noticed that with a rotor of this kind, which is composed of solid discs, the greatest stress is roughly between 40% (Fig. 5) and 60% (Fig. 6) lower than for rotors machined from the solid or for shrunk-on discs. This fact will again be important when considering the choice of material and the bursting speed.

HP and IP Rotors, Including Temperature Effects

Figure 8 shows the isotherms in a welded h.p. rotor under conditions of full load. Here one can see the characteristic feature of steady-state operation that the isotherms run almost perpendicular to the axis of rotation, and on the basis of the isotherm distribution one can predict that the thermal stresses will be very small compared to the stresses caused by rotation. In this example they in fact amount to only some 5 to 10% of the mechanical stresses. In contrast to the cold low-pressure section, the mechanical design of rotors exposed to high temperatures includes their behaviour in relation to time. Because of creep phenomena, which will be discussed in more detail in the next section, the material ages in the course of time. This ageing process is a function of the material, temperature and stress, as well as time, and therefore in order to assess the suitability of a design one must know all these parameters, i.e.

– the behaviour of the material as a function of loading, temperature and time,

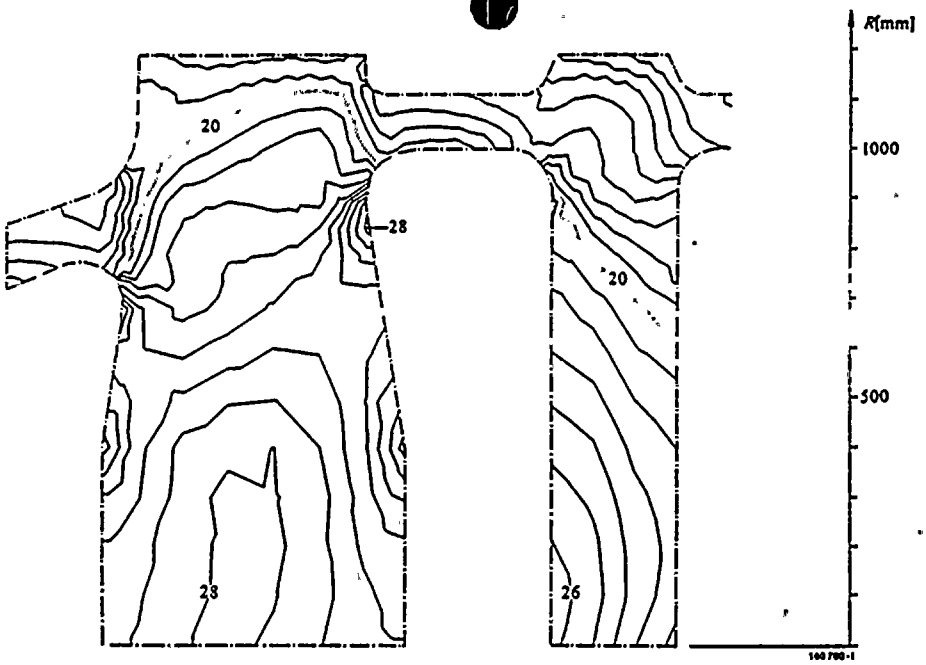

Fig. 7 – Combined stress field in a welded drum rotor as shown in Fig. 1c

Values 20 to 28 kgf/mm².

– the isotherm distribution in the rotor, and
– the stresses in the rotor.

An example of a detailed study of a high-pressure blade fixing is shown in Fig. 9. Using photoelastic techniques, the edge stresses in the lateral grooves are determined under different loads and added as supplementary information to the results of a refined stress calculation (Fig. 9). In this way, together with allowance for the behaviour of the material and stringent production quality control, it is possible to guarantee the performance of the rotor over many years.

The Rotor Material

High-Pressure and Intermediate-Pressure Rotors

The rotors of modern large steam turbines are all of ferritic material. This is related to the fact that for conventional plant the world over the live steam temperature has become established at 538 °C. With this material one can expect good long-time properties, no softening, little creep, uniform heat treatment, adequate long-term ductility, low notch sensitivity and good resistance to scale.

Nuclear power stations at present do not raise any problems of temperature because the turbines run on saturated steam, and even the high-temperature reactors for large power stations will not exceed the live steam temperature of conventional plant, at least in the near future.

Figure 10 shows two typical rotor steels [11] used for h.p. and i.p. turbines. To allow internationally consistent comparisons, the long-time rupture values for 100000 hours are taken as a basis for mechanical design purposes.

The following remarks survey briefly the behaviour of rotor materials under the influence of temperature, stress and time.

If a test bar is subjected to a load σ_0 and at the same time a temperature T_0, it will in time undergo plastic elongation (creep) and finally break. For the same loading the bar will fail earlier with a higher test temperature $T_1 > T_0$ than with a lower temperature.

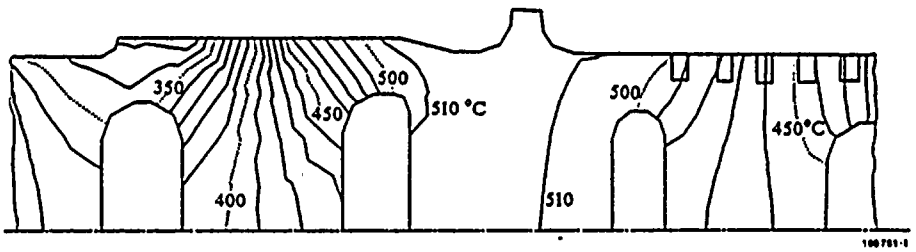

Fig. 8 – Isotherm distribution in a welded h.p. rotor

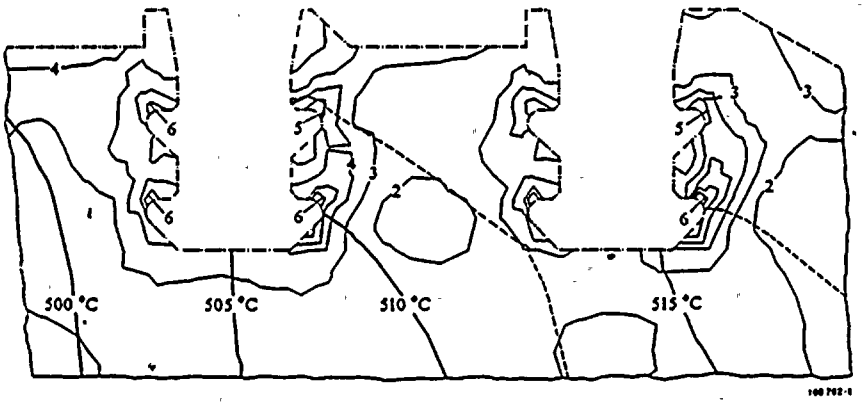

Fig. 9 – Combined stresses in the grooves of h.p. blade fixing

The figures denote the von Mises combined stress in kgf/mm².

The creep process is illustrated in Fig. 11. We can distinguish three main phases of creep, primary (I), secondary (II) and tertiary (III), in which the bar rapidly reaches breaking point. All high-pressure and intermediate-pressure rotors operate within the secondary phase, and the designer has to make sure that his design has an adequate reserve with respect to the tertiary stage. In the secondary phase the rate of creep $\dot{e} = de/dt$ is constant, which in practice makes it easier to assess the rotor after a long period in service. Every time the turbine is inspected, specially provided control diameters are measured and the results compared with measurements of previous years. Here, however, account must be taken of the fact that the creep rate within a disc varies widely from inside to outside owing to variations in the stress.

Fig.10 – Long-time rupture curves σ_{BR} in kgf/mm² and chemical composition of steels 24 CrMoV 55 and 21 CrMoV 511

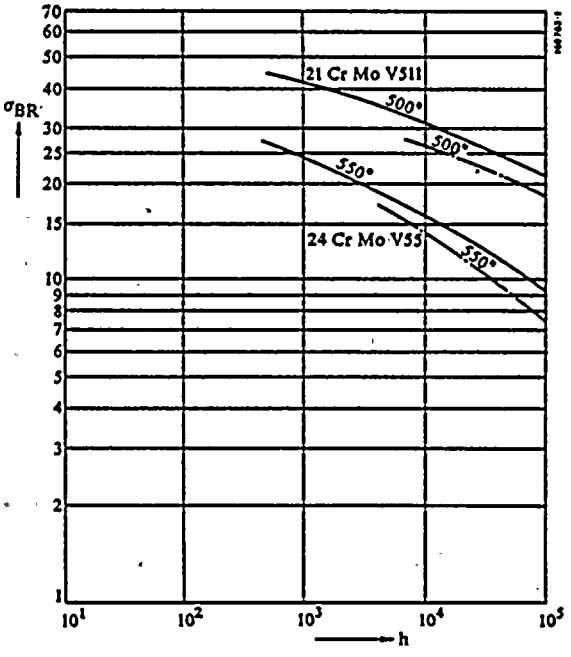

Low-Pressure Rotors

Whereas for high-temperature conditions the number of different rotor materials used by the various manufacturers is limited, the selection of materials for low-pressure rotors is much wider. This is not all that remarkable when one remembers the variety of l.p. rotor designs, because the material is principally matched to the different stress conditions of the individual types of construction. Furthermore, because these rotors are essentially cool, the factors governing the choice of material will only be the yield point, ultimate strength, elastic limit and notch toughness. Here it is assumed that the rotor operates in the upper part of the notch toughness range, i.e. the fracture appearance transition temperature is below the operating temperature.

Recently, and not the least of the reasons being several cases of explosive failure of solid and shrunk-disc rotors, which also extended to nuclear stations [10], there has been a tendency to base the choice of material on additional criteria in order to avoid such instances of brittle fracture. For this, the rotor is considered from the standpoint of fracture mechanics, the aim being to arrive at appropriate values of crack resistance and rate of propagation for subcritical crack growth. Without going into the fundamentals of fracture mechanics—the subject

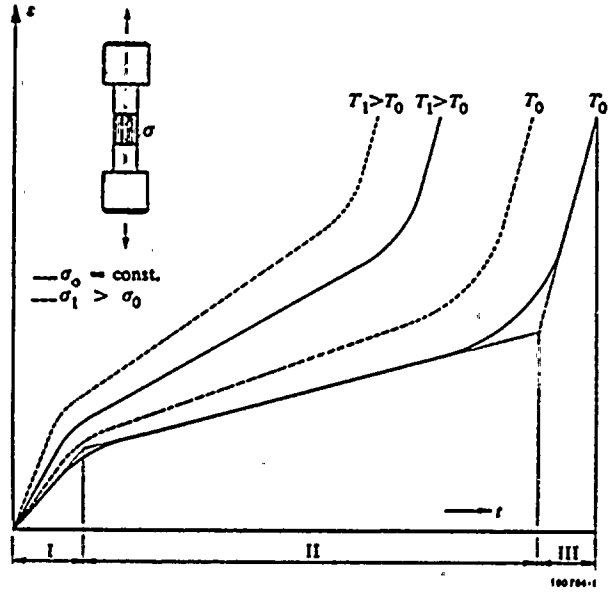

Fig. 11 – Creep curves for different temperatures and loads (schematic)

is treated in [12] and [13], for example—it should be mentioned that this aspect of mechanics was originally evolved for high-strength, relatively brittle materials. However, it is only suitable for describing a crack which already exists, and takes no account of the actual formation of the crack. At the same time it should not be forgotten that turbine rotors consist of ductile materials which have the ability, if need be, to flow locally and disperse stress peaks, thus preventing cracks from forming, or at least greatly delaying their onset.

It can, of course, happen that there is some justification for examining a rotor from a fracture mechanics viewpoint. This will always be so if, because of the high level of disc stresses, one has to resort to high-strength materials or when, as in the case of solid low-pressure rotors, the large dimensions make it very difficult to detect faults inside the forging. It may then be of advantage to assume a fault of a certain size in a certain position and check to see what the consequences might be in the course of time.

Bursting Speed

In recent years, and initially at the request of the US Atomic Energy Commission, manufacturers of large turbines for nuclear power plant have had to analyse the extent of damage to the turboset in the event of total failure of all control and safety systems. In this hypothetical situation, rejection of the electrical load would cause the rotor speed to run away, possibly resulting in explosive failure.

Our own studies have shown that h.p. and i.p. rotors have a much higher bursting speed than l.p. rotors. The reason for this is that the high and intermediate-pressure rotors stretch radially less than the low-pressure rotors, and while the material characteristic governing bursting is the yield point, h.p. and i.p. rotors are generally designed to withstand long-time failure. Since the value for long-time failure is only a fraction of the corresponding yield point, depending on the temperature, these rotors have a larger reserve with respect to the bursting speed than do l.p. rotors.

In order to study the behaviour of different disc designs in relation to the bursting speed we again use the disc of uniform width as a starting point. Grammel has shown [14] that the mean tangential stress in the disc is suitable as a measure of the resistance to explosive failure. The mean tangential stress σ_{tM} is given by

$$\sigma_{tM} = \frac{\int_{r_1}^{r_2} \sigma_t \, dr}{r_2 - r_1} \tag{16}$$

and can be written in dimensionless form as follows:

$$S_{tM} = \frac{\int_{r_1}^{r_2} \frac{8\,\sigma_t}{\varrho\, r_2^2\, \omega^2\, (3+\nu)}\, dr}{r_2 - r_1} \tag{17}$$

For σ_t we then use Eq. (3) for a solid disc and Eq. (5) for a perforated disc. If we now write the ratio of the mean tangential stress S_{tML} of the perforated disc to the mean tangential stress S_{tMV} of the solid disc, we have

$$\frac{S_{tML}}{S_{tMV}} = 1 + \frac{r_1}{r_2} + \left(\frac{r_1}{r_2}\right)^2 \tag{18}$$

The ratio of the bursting speeds of perforated disc to solid disc is then described by

$$\frac{n_{BRL}}{n_{BRV}} = \sqrt{\frac{1}{1 + \frac{r_1}{r_2} + \left(\frac{r_1}{r_2}\right)^2}} \tag{19}$$

Equations (18) and (19) are shown graphically in Fig. 12. As examination will quickly show, for $r_1/r_2 \to 1$ they will of course provide the bursting speed ratio for the thin ring.

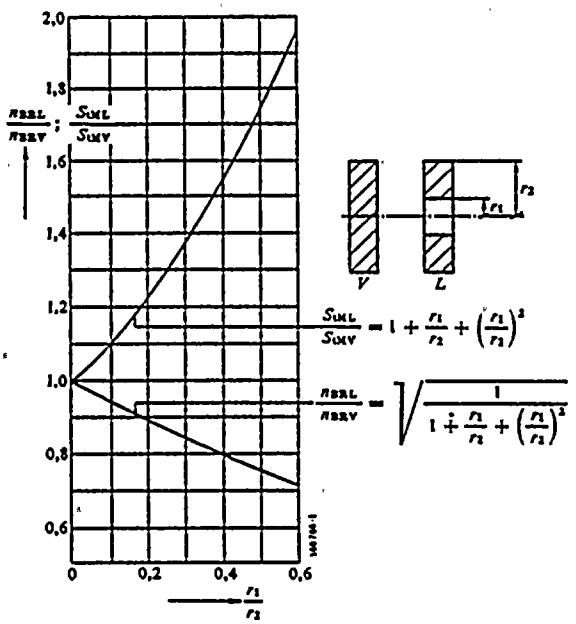

Fig. 12 – Ratios of mean tangential stress and bursting speed for perforated and solid discs

Figure 13 shows in qualitative terms the behaviour of two different l.p. rotor constructions at elevated speed. For the same size, blade tension and operating speed, the tangential stress for the drum rotor will follow curve 1. The same applies to the disc rotor, but at the bore diameter chosen this rotor shows a stress roughly double that of the drum rotor. In the elastic region there is proportionality between the stress and the square of the speed. If the speed is raised relative to the normal speed by a factor of 1·4, for example, the stresses increase by a factor of 1·96 (curve 2). The inner portion of the perforated disc is then already beyond the yield point, and the corresponding zone relaxes.

Owing to plastic deformation, therefore, the elastic curve 2 gives way to curve 2′ and the parts of the disc which are still elastic are thus subjected to additional stress. According to what has been said so far, a measure of the reserve with respect to fracture is the ratio of the yield point to the mean tangential stress, i.e. essentially the area in Fig. 13 contained between curves 1 and the yield point. The root of this area ratio represents the relationship of the bursting speed of the two designs shown in Fig. 13. If one wishes to compensate the disadvantage of the lower fracture speed of a perforated disc by using more highly tempered material, the increase in yield point required for a perforated disc can also be found with Eq. (18) (Fig. 12). It can be seen that with the radius ratios occurring in practice it is difficult to achieve a perforated disc of such a quality that it is equivalent to a solid disc as regards its bursting speed. This would mean high-strength material has to be used, with the consequent higher risk of brittle fracture.

Fig. 13 – Behaviour of two types of l.p. rotor at elevated speed

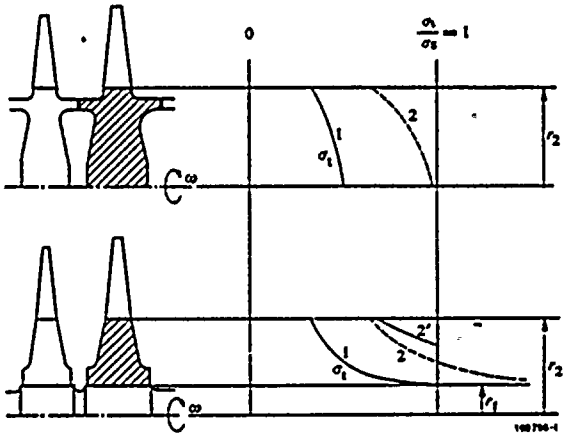

Outlook

As mentioned earlier, the unit capacity of large steam turbosets will continue to rise in the foreseeable future, and hence influence the demands made of the rotors. A decisive, and to some extent limiting, factor over the past decade was the final stage, which if the vacuum was good had to handle enormous flow volumes. All manufacturers of steam turbines therefore carefully developed longer final blades and introduced these to the market. But longer blades also means a larger rotor diameter, accompanied by higher centrifugal loadings on both blades and rotor. To keep stresses below the limit, the speed of the machines was halved. The technique employed in the USA was to run the high and intermediate-pressure sections at the full speed of 3600 rev/min, and combine the low-pressure units with a 4-pole generator on a second shaft string running at 1800 rev/min. Europe later adopted the idea of the half-speed machine, although in

single-shaft form and only for nuclear plant. By halving the speed in this way, and at the same time doubling the size, the stresses in full-speed and half-speed machines were kept the same, but the corresponding exhaust area of the final blades increased fourfold.

A feature of recent years has been a growing worldwide shortage of cooling water [15]. In the industrialized countries, and these if only because of their power distribution networks are the potential buyers of large machines, it is becoming no longer possible to use fresh water for cooling purposes. Future large power stations will therefore be equipped mainly with wet or dry cooling towers, which means the turbine vacuum will be relatively poor and the steam exhaust volume correspondingly smaller. It may thus well be that the final blade lengths and l.p. rotor dimensions customary today will be adequate for some time to come, without being tied to half-speed l.p. sections because of the stresses, even with large capacities. It is likely that large machines for nuclear power stations, with poor vacuum, will also be built for full speed and still be able to cope with the stresses in the blades and rotor.

The possibility of making the l.p. rotor relatively small also improves the chances of the solid-rotor design to some degree. Great advances in forging technology have been made over the past few years, and this has increased confidence in the use of forged one-piece shafts. Finished weights of over 200 t have been achieved to date. These rotors require an ingot weighing more than 400 t and with the associated risks can be produced only in Japan and the United States. It is improbable that the steelworks will contemplate a further increase in rotor size, with the correspondingly heavy investment needed to deal with larger ingots, because the market for these large forgings is too restricted. The concept of the large one-piece rotor can therefore be extrapolated into the future to only a limited extent.

The situation is slightly different for the high-pressure section. On the assumption that future nuclear power stations will also operate with steam conditions such as are found today in conventional plant (150 to 250 bar, 538 °C), the very size of the l.p. rotor could present a stress problem. Overcoming this can be approached in two different ways: the material and the design.

There is no likelihood in the near future of finding a different material for h.p. rotors which has substantially better long-term properties and does not forfeit the advantages of the low alloy steels used at present. Much more probable is that stresses in the h.p. rotor can be kept in check through suitable design: the large steam turbine today is quite clearly following the path taken many years ago by the gas turbine towards cooling the rotor by means of steam. The designer thus has at his disposal a design concept sufficiently flexible to allow him an adequate margin of safety in designing rotors for the high-pressure section as unit capacities continue to rise.

Symbols

E = Modulus of elasticity
L = Perforated disc
S_r = Dimensionless radial stress
S_t = Dimensionless tangential stress
S_{tM} = Dimensionless mean tangential stress
S_V = Dimensionless equivalent voltage
T = Temperature
U = Radial displacement
V = Solid disc
a = Thermal conductivity
c = Specific heat of rotor material
n_{BR} = Bursting speed
r = Considered disc radius
r_1 = Inner radius of perforated disc
r_2 = Outer radius of disc
Δr = Degree of shrinkage
$\frac{\Delta r}{r_1}$ = Relative degree of shrinkage
t = Time
ε_r = Radial expansion
ε_t = Tangential expansion
λ = Conductivity of rotor material
ν = Transverse contraction ratio
ϱ = Specific mass of disc material
σ_r = Radial stress
σ_{r1} = Shrinkage force
σ_{r2} = Blade tension applied at radius r_2
σ_t = Tangential stress
σ_{tM} = Mean tangential stress over meridional area of blade
σ_z = Axial stresses in rotor
ω = Angular velocity of rotation
ω' = Overspeed
ω^* = Lift-off speed

Indices

W = Central shaft
S = Disc
0 = Standstill

Bibliography

[1] *A. Lüthy:* Some advantages of welding turbine rotors. Weld. J. June 1968.

[2] *C.B. Bienzeno, R. Grammel:* Technische Dynamik, vol. II, Springer 1953.

[3] *W. Traupel:* Thermische Turbomaschinen, vol. II, Springer 1960.

[4] *K. Löffler:* Die Berechnung von rotierenden Scheiben und Schalen. Springer 1961.

[5] *A. Bald:* Besonderheiten grosser Nassdampfturbosätze. Mitt. Vereinig. Grosskesselbesitzer *52* 1972 (4).

[6] *O.C. Zienkiewicz:* The finite element method in structural and continuum mechanics. McGraw-Hill, London 1967.

[7] *B. Baule:* Die Mathematik des Naturforschers und Ingenieurs, vol. IV. Hirzel 1952.

[8] *H. Leipholz:* Festigkeitslehre für den Konstrukteur. Springer 1969.

[9] *H.D. Emmert:* Investigation of large turbine spindle failure. ASME Paper *55* – A 172.

[10] *D. Calderon:* Steam turbine failure at Hinkley Point. Proc. Inst. mech. Engrs *186.*

[11] Stähle für grössere Schmiedestücke (Gütevorschrift). Stahl-Eisen-Werkstoffblatt *550* – *57.*

[12] *K. Heckel:* Einführung in die technische Anwendung der Bruchmechanik. Hanser 1970.

[13] *D. Radaj:* Grundlegende Beziehungen der linear-elastischen Bruchmechanik. Schweissen u. Schneiden *23* 1971 (10).

[14] *R. Grammel:* Die Erklärung des Problems der hohen Sprengfestigkeit umlaufender Scheiben. Ingenieur-Archiv *16* 1947 (1).

[15] *H. Flohn, D. Henschler, H. Schuller:* Der Wasserhaushalt der Erde. Aus: Mensch und Umwelt. Tech. Rdsch. *64* 1972 (47).

BBC
BROWN BOVERI

BBC Brown, Boveri & Company, Ltd.
CH - 5401 Baden/Switzerland

Printed in Switzerland (7404-1000-0)
Classification No. 01010